Fast and complete degradation of Congo red under visible light with Er^{3+} and Nd^{3+} ions doped TiO_2 nanocomposites

Himanshu Narayan,[1] Hailemichael Alemu,[2] Daniel N. Alotsi,[2] Lebohang Macheli,[2] Madhavi Thakurdesai,[3] Sandesh Jaybhaye,[4] Arvind Singh[5]

[1]Department of Physics and Electronics, National University of Lesotho, Roma 180, Lesotho; [2]Department of Chemistry and Chemical Technology, National University of Lesotho, Roma 180, Lesotho; [3]Department of Physics, Birla College, Kalyan 421 304, India; [4]Department of Chemistry, Birla College, Kalyan 421 304, India [5]National Centre for Nanomaterials and Nanotechnology, University of Mumbai, Mumbai 400 098, India

Abstract

We report fast and complete destruction of the dye Congo red (CR) under visible light in the presence of Nd^{3+} and Er^{3+} doped TiO_2 nanocomposites (NCs). TiO_2 NCs with general composition $TiO_2[R_2O_3]_x$, {x=0.1, 0.2; R≡ Nd, Er} and particle size 12-16 nm were synthesized through co-precipitation/hydrolysis (CPH). A set of similar composites was also prepared through solid state reaction (SSR) route, which produced 31-47 nm particles. After characterization, visible light photocatalytic activity of all the samples was recorded for the degradation of CR. NCs with molar concentration x=0.2 of both doping types produced close to 100% degradation in 180 min. The apparent rate constant (k_{obs}) was found to be 2.91×10^{-2} min^{-1} and 2.36×10^{-2} min^{-1}, for these Nd^{3+} and Er^{3+} doped NCs, respectively. The other NCs with x=0.1, also showed significant degradation of CR, but the samples prepared through SSR performed worse. The excellent degradation obtained with the NCs may be attributed to their small particle size. Moreover, the doping of Nd^{3+} and Er^{3+} ions further supported the photocatalysis through formation of intermediate energy levels within the band gap of TiO_2. These new levels not only acted as electron traps for efficient suppression of the undesired e^-/h^+ recombination, but also facilitated to a certain extent the absorption of visible irradiation.

Introduction

Discharge of waste products from various industries leading to environmental pollution is a worldwide problem of great concern. Waste products, whether solid or non-solid, influence the natural processes of the ecosystem. The most undesirable fate of almost all waste products, especially the water-soluble ones, is that they end up polluting the water systems. Currently the coloration of water in rivers and streams is due to the large amounts of colored organic effluents (mainly the synthetic dyes) discharged from industries, such as the textile, rubber, cosmetic, paper industries, etc., where coloration of products is of great importance. As a result, such industries are major contributors to environmental pollution.[1-5]

More than 60% of the world production of dyes is utilized in textile industries, and during the processing about 10-20% is discharged as effluents.[1,2] These dye effluents distract the food web in water because their intense color reduces the light transmission, and thus inhibits the growth of most aquatic plants, as well as raises the biological oxygen demand (BOD) and the chemical oxygen demand (COD) in the water. Furthermore, they are potentially carcinogenic and mutagenic, and may also cause allergenic dermatitis and skin irritation even in small amounts.[1,2] Because of these reasons, the discharge of dye effluents requires special handling and proper and effective treatments, not just for the possible reuse of disinfected water, but also to promote a cleaner and healthier environment.

Photocatalytic destruction of organic pollutants based on semiconductor photochemistry (advanced oxidative processes such as heterogeneous photocatalysis) has been an attractive method since the 1970s and in recent years, this method has been investigated by various groups for degrading synthetic dyes. In heterogeneous photocatalysis, photo-induced molecular reactions or transformations occur at the surface of a catalyst. The process involves initial absorption of photons by the catalyst substrate or the pollutant molecule in order to produce highly reactive chemical species. Depending on where the first excitation takes place, photocatalysis can be divided into two fundamental processes: the catalyzed photoreaction and sensitized photoreaction, respectively. The first process takes place when the initial excitation occurs in the catalyst particle followed by electron or energy transfer from the catalyst to the pollutant molecule and the second, when an adsorbed molecule gets photo-excited initially leading to an interaction with the catalyst.[2,5-7]

Titanium oxide (TiO_2), a wide band gap (3.2 eV) semiconductor with several attractive optical and electronic properties, has been recognized as the most effective photocatalyst for the purpose of degradation. When TiO_2 is irradiated with ultraviolet (UV) radiations of suitable wavelengths (<390 nm), the electrons in the valence band (VB) of the semiconductor get excited and promoted to the conduction band (CB). Consequently, pairs of negative-electron and positive-holes (e^-/h^+) are created. The generation of e^-/h^+ pairs is a crucial feature that initiates primary reactions involving the hydroxide ions, water and oxygen to form highly active species (e.g. the hydroxyl radicals OH* and superoxide anion radicals O_2^{2-}). These species interact directly with the pollutants leading to their oxidative degradation.[5-7] In this mechanism, obviously the band gap of the photocatalyst is the controlling factor.

Another and perhaps more important mechanism so far as the visible light induced photocatalysis is concerned, is that of photosensitization.[8-10] In this process, the pollutant molecule (e.g. dye molecule) must initially get adsorbed onto the surface of TiO_2 and start absorbing visible radiations. This eventually results in the electrons of adsorbed molecule being photochemically excited and finally transferred to the catalyst particle. This transfer produces superoxide anion radicals from reduction of the molecular oxygen and, at the same time, a cation radical is also produced from the pollutant molecule. Both of these radicals lead to the degradation of other pollutant molecules. In this case, the degradation of the organic pollutant is dependent on the effective

Correspondence: Himanshu Narayan, Department of Physics and Electronics, National University of Lesotho, Roma 180, Lesotho.
E-mail: h.narayan@nul.ls

Key words: titanium oxide, rare-earth ions, photocatalytic degradation, recombination.

Acknowledgments: the authors would like to thank Ms. Renuka Jaiswal for all her help in carrying out various experiments. The authors from India are grateful to Prof. DC Kothari, Head, Department of Physics; and Coordinator, National Centre for Nanomaterials and Nanotechnology, University of Mumbai, Mumbai, India for his encouragement and support.

Received for publication: 28 October 2011.
Revision received: 1 December 2011.
Accepted for publication: 14 December 2011.

Nanotechnology Development 2012; 2:e
doi:10.4081/nd.2012.e2

surface area of the catalyst particle.

Among the chemically active species generated during these processes, the holes (h^+) and the hydroxyl radicals are the most influential in a photocatalytic oxidation process. The holes play a key role in the formation of the OH* radicals, which are strong oxidation agents significant in the process of degradation. Additionally, the holes may directly react with the pollutant molecules leading to their degradation. Therefore, it may easily be concluded that suppression of recombination between the photogenerated e^-/h^+ pairs is crucial for better photocatalytic efficiency.[9,11,12]

It is clear from the above discussion that the photocatalytic performance of a material depends primarily on its band gap and the particle size. The band gap is important because it determines the range of appropriate wavelengths required for photo-excitation. The wide band gap of pure TiO_2 restricts the useful regions of the spectrum to under 390 nm (absorption-edge or cut-off wavelength, λ_{cutoff}). Thus, visible light induced photocatalysis through photo-excitation is not feasible unless the pure material is modified in such a way that the band gap is narrowed (leading to a red-shift of λ_{cutoff} towards the visible regions). It has been reported that band gap can be narrowed through doping of some transition metals[13,14] as well as some narrow-band semiconductors.[15,16] Smaller particles, on the other hand, can increase the specific surface area of the catalyst to facilitate additional photosensitization and hence produce improved degradation. However, there is a limit: particles with less than about 10 nm size may retard the degradation instead of enhancing it, because such a small size (i) may assist detrimental e^-/h^+ recombination due to the smaller mean-free-path, and (ii) may be associated with wider band gaps (quantum size effect) causing λ_{cutoff} to blue-shift away from the useful visible regions.[9,10]

Our recent investigations have reasonably established that even when the band gap is not substantially narrowed due to doping of TiO_2, photocatalytic degradation can still be carried out under visible light, primarily through the process of photosensitization. The latter is supported by smaller particle size, preferably in the range 10-20 nm.[9,10,12] Also, appropriate doping with metal ions can additionally improve the degradation through effective control of the unwanted e^-/h^+ recombination. Under these considerations, we have noted that rare-earth ions could be a suitable choice as dopants.[9] In the recent past, some research has been reported on rare-earth ions doped TiO_2 photocatalyst materials.[17-22] Apart from facilitating efficient suppression of e^-/h^+ recombination, some rare-earth ions, due to their unique electronic structure, may also induce indirect band-gap modification such that visible light photocatalysis is supported. However, the literature is still not sufficient and this specific field of research is still open to a number of new possibilities. Extending our work along these lines, we report the photocatalytic activity of Nd^{3+} and Er^{3+} doped TiO_2 nanocomposites. The most interesting part is that some of these photocatalytic materials have produced close to 100% degradation of the dye Congo red at a very fast rate.

Materials and Methods

Materials synthesis

Neodymium nitrate (99.9% metal basis), erbium nitrate (99.9% metal basis), oxides of neodymium and erbium, isopropanol and titanium(IV)-butoxide [$Ti(OBu)_4$] (97% reagent grade) were supplied by Aldrich Chemical Corporations, while ammonium hydroxide was obtained from Shalom Laboratory Supplies. Congo red was procured from E. Merck Co. (Darmstadt, Germany).

Neodymium oxide and erbium oxide doped titanium oxide nanocomposites $TiO_2[R_2O_3]_x$, {x=0.1, 0.2; R = Nd, Er} were synthesized through the preparation methods reported earlier.[9,10] The method of synthesis for the nanocomposites (NCs) was co-precipitation followed by hydrolysis (CPH), and for the polycrystalline (PC) samples, the solid state reaction (SSR) route was adopted. The CPH method initially involved the nitrate salt of each dopant dissolved in isopropanol through stirring and heating at around 55-65°C. Then 3.5 M ammonium hydroxide (NH_4OH) was prepared in isopropanol and 10 mL of this solution was added to the solution of metal nitrate to affect hydrolysis. This raised the pH of the nitrate solution to around 6.5 where the nitrate precursors were precipitated. Approximately 10 mL of distilled water was added drop-by-drop to the solution and the solution was further agitated for 30 min.

A mixture of $Ti(OBu)_4$ and isopropanol was prepared in the ratio of 1:2 by weight and added drop-wise to the co-precipitated metal nitrate precursor for controlled hydrolysis and agitation of the mixture was continued for 60 min while slowly adding distilled water to prevent the setting of the solution. The doped NCs were then recovered from the solution by drying at room temperature followed by calcination at 400°C for a maximum period of 3 h.

TiO_2 PC composites were also synthesized with the SSR method. This involved dissolving the respective oxides in ethanol followed by additions of a stoichiometric amount of commercial TiO_2, while continuously stirring. The solution was then further agitated, dried, ground and calcined for nearly 3 h at 600°C. This method produced particles of larger size.

Measurements

The transmission electron microscopy (TEM) was carried out on a Philips CM200 TEM instrument (FEI Co.). Using the same unit, the selected area electron diffraction (SAED) patterns were also recorded. Powder X-ray diffraction (XRD) patterns were recorded with Shimadzu D6000 diffractometer (Shimadzu, Japan) using CuKα radiation (λ= 1.5406 Å). Fourier transform infra-red spectroscopy (FTIR) was performed on a Jasco FTIR 4100 set up (Jasco) and Raman spectra with an inVia Raman microscope (Renishaw) with a source wave length of 514 nm. Diffused reflectance spectroscopy (DRS) was carried out to record the absorption spectra of the samples using a Varian CARY 5000 UV-VIS-NIR absorption spectrometer (TNLabs).

The visible-light photocatalytic degradation was carried out using a cost-effective photoreactor organized in the laboratory.[10] In this scheme, a 1 L glass beaker with a magnetic bar was placed on a magnetic stirrer. A smaller 250 mL beaker was placed inside it to house the light source (fluorescent lamp) so that it was separated from the water. The smaller beaker was held in place inside the bigger one using a ring attached to a stand fitted on the top. After filling about 750 mL of the experimental solution (CR solution along with the photocatalyst), the smaller beaker glass was sealed with parafilm where it touched the top outer rim of the large beaker. A compact fluorescent lamp (Philips) held in place with a 3-pronged clamp was finally placed in the middle of the 250 mL beaker inside the experimental solution so that it was not touching the sides or the bottom of the beaker.

Prior to the actual degradation experiments, a series of control and optimization experiments were performed. The absorbance of an experimental solution was recorded (i) under light irradiation but without any photocatalyst, and (ii) in the dark with a solution that contained photocatalyst. It was established that the catalyst and light alone could not produce any meaningful degradation. On the other hand, the amounts of photocatalyst and CR in the experimental solution were optimized for best results. Accordingly, an experimental solution (750 mL) containing 5.5 $mg.L^{-1}$ of CR, and 250 $mg.L^{-1}$ of photocatalyst sample were placed in the photoreactor, and the fluorescent lamp was turned on to initiate photocatalysis under visible light. The solution was kept stirred throughout the duration of the experiment. At predetermined times (every 30 min up to 180 min), 3 mL aliquots of the dye solution were taken from the photoreactor and centrifuged for about 3 min. The absorbance of the centrifuged solution was recorded at λ=498

nm (absorption peak of CR) using a UV-Vis Shimadzu 1201 spectrophotometer. In the entire photocatalysis experiments, the instrument was baseline corrected with distilled water. For a better analysis of the results, for every solution from the centrifuge, the entire useful range of the spectrum (400-600 nm) within which the absorption peak for CR is expected, was scanned and thus the degradation curves were obtained.

Results and Discussion

TEM was used to examine the particle size, crystallinity and morphology of samples. TEM bright field image of $TiO_2[R_2O_3]_x$, {R ≡ Nd, Er} for x=0.1 NCs is shown in Figure 1. The particles are mostly spherical or ellipsoidal in shape and the approximate size of the particles varies from about 9 to 17 nm for Er^{3+} doped, and from about 8 to 16 nm for Nd^{3+} doped NCs. The corresponding SAED patterns of the NCs are shown in Figure 2. These patterns for both the NCs exhibit low intensity spots located on the ring pattern. This may be attributed to the reduced crystallinity of the samples, which was confirmed from XRD results as discussed below.

Figure 3 shows the XRD results for both the NC (CPH synthesized) and PC (SSR prepared) samples of $TiO_2[R_2O_3]_x$, {x=0.1, 0.2; R ≡ Nd, Er} composites. The most prominent peak around 2θ = 25.2° in all the plots corresponds to the (101) peak of anatase, which is obviously the dominating TiO_2 phase in all the samples. Some other expected anatase peaks are also visible: around 2θ = 37.7°, 47.9°, 53.8° and 55.0° corresponding to the (004), (200), (105) and (121) reflections, respectively, especially in the data for PC composites. However, compared to the XRD data for pure anatase, all these peaks are slightly shifted from their respective 2θ values. For example, the most significant (101) peak occurs at 2θ = 25.7° in pure anatase, but in the composites it is observed at 2θ = 25.5° and 25.3° (for x=0.1 and 0.2 Nd^{3+} doping, respectively) and at 2θ = 25.2° (for both x=0.1 and 0.2 Er^{3+} doping). This is a clear indication that the dopant ions occupied the lattice sites resulting in small deformation of the crystal structure. In addition to this, the presence of very intense peaks at 2θ = 20.6°, 29.3°, 34.0°, 43.8°, 48.8° and 58.0° associated with the (211), (222), (400), (341/431), (440) and (622) orientations, respectively, of the cubic Er_2O_3, point to the presence of this phase also in the composites doped with Er^{3+} ions. Similarly, the XRD data for the Nd^{3+} ions doped samples indicate the presence of hexagonal Nd_2-O_3 phase in the composites because of the occurrence of significant peaks at 2θ = 27.6°,

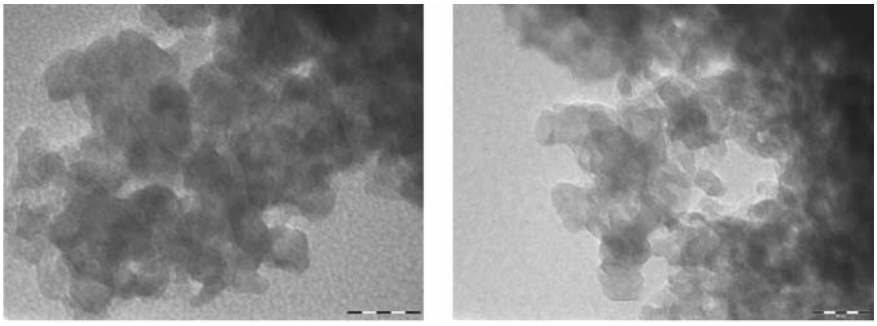

Figure 1. Typical TEM images of (a) x=0.1 Er^{3+} doped, and (b) x=0.1 Nd^{3+} doped NC. The scale in all pictures is 20 nm.

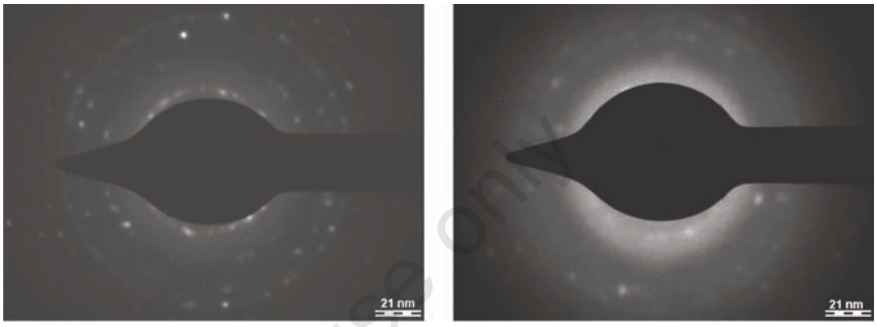

Figure 2. Selected area electron diffraction images of (a) x=0.1 Er3+ doped, and (b) x=0.1 Nd^{3+} doped NC.

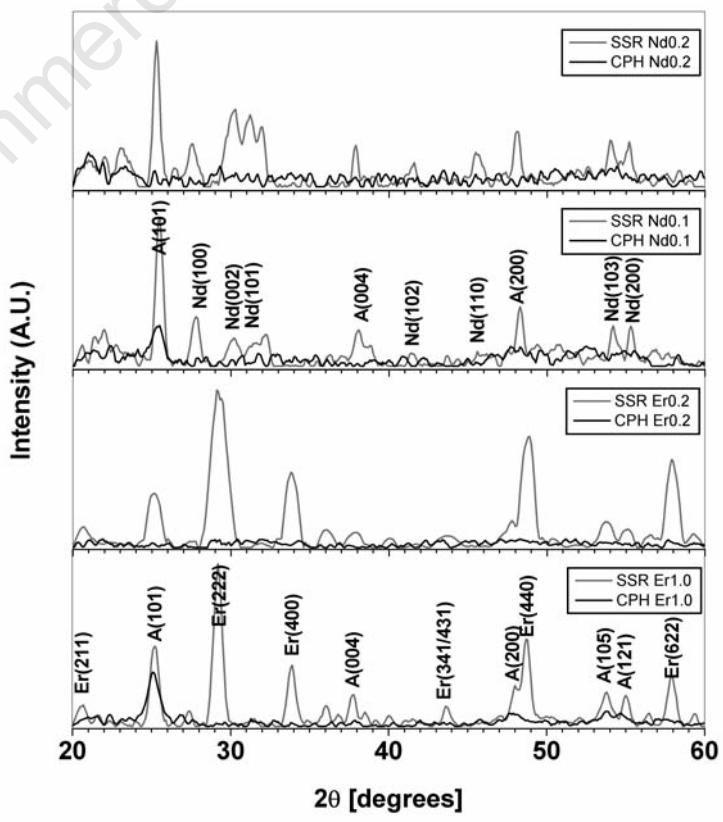

Figure 3. X-ray diffraction patterns of doped TiO_2 composites. Peak positions for the anatase phase are shown with letter A, those for Er_2O_3 with Er and those for Nd_2O_3 with Nd.

30.2°, 31.2°, 54.1° and 55.2° associated with the (100), (002), (101), (103) and (200) reflections of that phase, respectively. Therefore, it may be concluded that the doped rare-earth ions do not just occupy the lattice sites, but part of them also go into the interstitial space. The oxide phase of the doped R_2O_3 is thus retained, probably in the form of interstitial clusters or islands. Nevertheless, the repeatability of XRD results confirmed that overall homogeneity of the composites was maintained during either of these two substitution processes. More importantly, however, the XRD patterns did not suggest formation of any new phase.

Most of the XRD peaks in the CPH NCs were highly broadened and/or merged with the peaks of other phases. An obvious broadening of the prominent peaks directly indicates the reduced particle size, which is also confirmed from the size estimation using XRD data. The Debye-Scherrer formula[9,10,12] was used to estimate the particle size from XRD data. The prominent peaks were fitted with a Gaussian profile and their FWHM was used in the calculations. The particle size for the x=0.1 doped samples was estimated around 13 nm (Nd^{3+} doped) and 16 nm (Er^{3+} doped) from the XRD data, which matches well with the size of about 12 nm and 14 nm, respectively, measured from TEM. Similarly, for the x=0.2 doped samples, the average size from TEM pictures were found to be around 15 and 12 nm, in agreement with the XRD particle size of 13 and 12 nm, respectively, for Nd^{3+} and Er^{3+} doped NCs. Table 1 lists all the particle sizes estimated from XRD data.

The Raman and FTIR spectra for the NCs are shown in Figures 4 and 5, respectively. In general, the Raman profiles obtained with our samples show five characteristic peaks at 144, 197, 399, 513 and 639 cm^{-1}, which may be associated with the anatase TiO_2. In a typical Raman spectrum, usually, the presence of anatase is identified by five distinct peaks at 151, 196, 409, 515 and 633 cm^{-1}, assigned to the E_g, E_g, $B1_g$, A_{1g} or B_{1g} and E_g modes, respectively.[23,24] However, apparently the peaks corresponding to E_g and B_{1g} modes are red-shifted to around 144 and 399 cm^{-1}, respectively. Such red-shifts may be explained on the basis of a phonon confinement model, and are associated with reduced particle size of the material under consideration.[9,23] This observation agrees with the XRD results for all the NCs. Furthermore, Raman spectroscopy results also indicate suppression of the Ti-O bonds due to doping. It can be observed in the FTIR spectra (Figure 5) on the other hand, that there are apparently multiple peaks in the region 420 cm^{-1} to 550 cm^{-1} which are usually associated with the various characteristic vibrational modes of Ti-O bonds.[24] However, in the FTIR spectra for doped samples, the intense peaks at wave number 492 cm^{-1} and 434 cm^{-1} are missing, and overall the peak intensity is reduced. This indicates that the dopants have suppressed the Ti-O bonds; an observation that was also supported by Raman results as mentioned earlier. The absence of characteristic vibration modes for Nd and Nd_2O_3 and for Er and Er_2O_3, in the Raman and FTIR spectra suggests that there was no segregation of these elements or corresponding oxides in the TiO_2 matrix, which also confirms the homogeneity of the samples. Neither the Raman nor the FTIR results show any new peak corresponding to either R-O or Ti-O bonds.

The absorption spectra obtained through diffused reflectance spectroscopy (DRS) showed marginal red-shifts in the values of absorption-edge, λ_{cutoff}, for all the composite samples. Compared to the value of λ_{cutoff}= 390 nm for pure anatase, the doped NCs had λ_{cutoff} values of 415 and 419 nm (for x=0.1 and 0.2 Nd^{3+} doping, respectively), and 416 and 422 nm (for x=0.1 and 0.2 Er^{3+} doping, respectively). Since the wavelengths used for irradiation during photocatalysis were larger than 420 nm, these red-shifts might not have significantly affected the degradation results. However, some small absorption peaks were also present in the visible regions of the spectra, which could have contributed to the photocatalysis under visible light. Among these, the peak at 587 nm for Nd^{3+} doped NCs, and the one at 522 nm for Er^{3+} doped NCs cannot be ignored. The 528 and 587 nm absorption peaks have already been reported and their appearance has been attributed to the formation of intermediate energy levels between the VB and CB of TiO_2 due to the 4f shells of Nd^{3+} ions.[23] In the same line, the absorption peaks at 489, 522 and 654 nm, observed with Er^{3+} doped NCs may also be associated with the formation of similar ener-

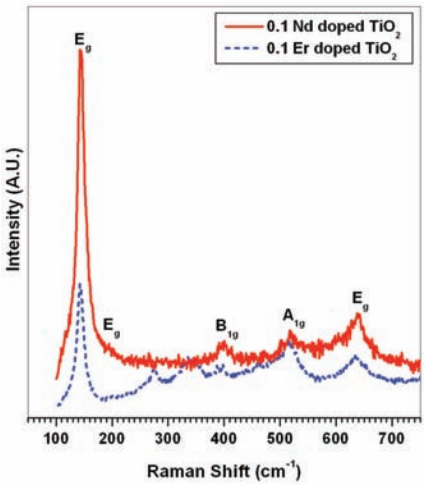

Figure 4. Raman spectra for Nd^{3+} and Er^{3+} doped TiO_2 NC samples.

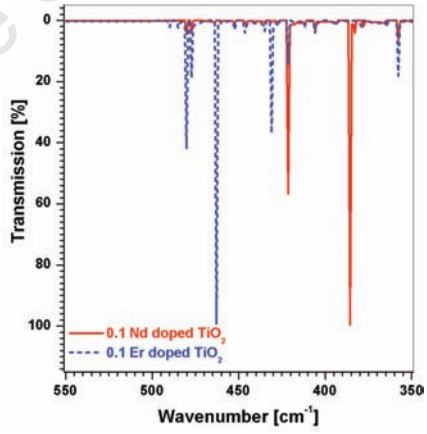

Figure 5. FTIR spectra for Nd^{3+} and Er^{3+} doped TiO_2 NC samples.

Table 1. Sample and experimental parameters.

Sample	x	Particle-size (nm)	k_{obs} (10^{-2} min^{-1})	$t_{1/2}$ (min)	C'_{180} (%)	Comments
Pure TiO_2 (anatase)	0.0	47	0.59 (0.38)	120	67	As received
CPH TiO_2.[Y_2O_3]x	0.1	16	2.74	24	91	Ref. [9]
	0.2	19	2.62	23	95	Ref. [9]
CPH TiO_2.[Nd_2O_3]x	0.1	13	2.01 (3.58)	18	97	
	0.2	15	2.91 (2.91)	16	100	
CPH TiO_2.[Er_2O_3]x	0.1	16	1.03 (1.70)	20	90	
	0.2	12	2.36 (3.88)	11	99	
SSR TiO_2.[Y_2O_3]x	0.1	38	0.31	-	57	Ref. [9]
	0.2	41	1.20	50	60	Ref. [9]
SSR TiO_2.[Nd_2O_3]x	0.1	47	0.55 (0.75)	98	64	
	0.2	40	0.94 (1.66)	20	86	
SSR TiO_2.[Er_2O_3]x	0.1	36	0.32 (0.50)	>180	44	
	0.2	31	0.45 (0.69)	118	55	

* The quantities in the brackets in k_{obs} column are the initial values for apparent rate constants calculated using the first four points (*i.e.* up to 90 min of degradation).

gy levels in these composites.

The degradation of CR in terms of the relative percentage [$(C/C_0)\times100$] of the dye concentration after each 30 min up to 180 min is shown in Figure 6. For comparison, we have also included the results obtained with Y^{3+} doped NCs reported earlier by some members of our group.[9] Two important observations can be immediately deduced from this figure. First, that in less than 25 min, all the CPH catalysts degraded the CR dye to half of the initial concentration or more. This implies that, in general, the synthesized NCs are very fast catalysts. Second, that after about 120 min, a saturation level was apparently reached and no further significant degradation was produced. In other words, it meant that with a given photo-catalyst, the maximum achievable degradation was reached just in approximately 2 h. In comparison, the as-received anatase powder took more than 2 h to degrade CR to half of its initial concentration under the same experimental conditions.

Rate of degradation for all the catalysts was found to be of the first order. From a least-square regression of $\ln(C/C_0)$ *versus* time data, the apparent rate constant (k_{obs}) was estimated for the degradation with each of the samples. Plots of $\ln(C/C_0)$ *versus* time, along with the best-fit straight lines, are shown in Figure 7 for both types of doped NCs. In terms of the degradation after 180 min (C'_{180}) the best performing sample was Nd^{3+} doped (x=0.2) TiO_2 NC. The value of C'_{180} with this sample was close to 100%, marginally better than the Er^{3+} doped (x=0.2) TiO_2 NC that degraded about 99% of CR, in the same time period. The x=0.1 doped NCs for both doping types also degraded a significant amount of CR (C'_{180}= 97 and 90% was obtained with Nd^{3+} and Er^{3+} doped x=0.1 NCs, respectively). In general, therefore, these NCs seemed to be much better than the Y^{3+} doped NCs reported earlier, which could degrade about 95% (x=0.2) and 91% (x=0.1) of CR in 180 min.[9] The as-received anatase powder, on the other hand, could degrade only about 67% of CR after 180 min.

In terms of the rate constant also, the best photocatalyst was x=0.2 Nd^{3+} doped TiO_2 NC, with the value of $k_{obs}=2.91\times10^{-2}$ min^{-1}. The Er^{3+} doped NC (x=0.2) was next with $k_{obs}=2.36\times10^{-2}$ min^{-1}, although the initial rate of degradation (calculated using the linear fit to the first four points in the graph, *i.e.* up to 90 min of degradation time; Figure 7B) for this photocatalyst was much higher at 3.88×10^{-2} min^{-1}. Because of such a high initial rate, this NC degraded more than half of the initial CR concentration in only approximately 11 min ($t_{1/2}$) and nearly 98% in just 1 h.

For a better understanding of the results, the degradation of CR with each SSR prepared sample was also recorded following the same procedure. The degradation produced by these samples was nearly the same or worse than the as-received anatase powder, except for the one doped with x=0.2 Nd^{3+}, which performed better with C'_{180}= 86% and a rate of $k_{obs}=0.94\times10^{-2}$ min^{-1}. With this sample, half of the starting CR concentration was reached in approximatley 20 min ($t_{1/2}$) because the initial value of k_{obs}(= 1.66×10^{-2} min^{-1}) was much better than that of the pure anatase (0.38×10^{-2} min^{-1}).

If the experimental conditions remain unchanged, a combination of some crucial intrinsic properties of the composites determines the final degradation results. These are the particle size, the ability to control e^-/h^+ recombination, and the weight fraction of TiO_2 in the composite. Additionally, sensitivity of the composites under visible light also becomes important when the doping favors absorption of the latter. Obviously this and the e^-/h^+ recombination suppression efficiency are the two factors associated with the physical properties and weight fraction of the dopants. Smaller particles produce better degradation because of the large specific surface area available for photosensitization. However, for a given particle size, the net degradation produced by a composite sample after a certain time, in general, should be a result of the competition between the two fractions, the TiO_2 weight fraction (TWF) and the dopant weight fraction (DWF). Starting with the best performing NCs, i.e. the Nd^{3+} doped TiO_2, close to 100% degradation obtained with the x=0.2 doping may be attributed to the 15 nm average particle size and TWF = 49% of that NC. In comparison, the x=0.1 molar fraction of this doping type, even with a larger TWF (68%) and smaller average particle size (13 nm), produced 97% degradation after 180 min, which is marginally worse than the x=0.2 doping. Clearly, it may be associated with a slightly poorer inhibition of the e^-/h^+ recombination and a weaker sensitivity to visible light because of the smaller DWF of Nd^{3+} ions in the NC. In the x=0.2 Er^{3+} doped NC, an excellent degradation of 99% was observed after 180 min. This may be due to the smaller average particle size of 12 nm, even though the TWF in this NC was only about 45%. The x=0.1 Er^{3+} doped NC with higher TWF of 65%, on the other hand, produced only about 90% degradation in 180 min, apparently because it had a larger particle size of 16 nm as well as a smaller DWF (i.e. worse restriction of the e^-/h^+ recombination and lesser sensitivity to visible light) of Er^{3+} ions.

The importance of doping becomes clear when the above results are compared with

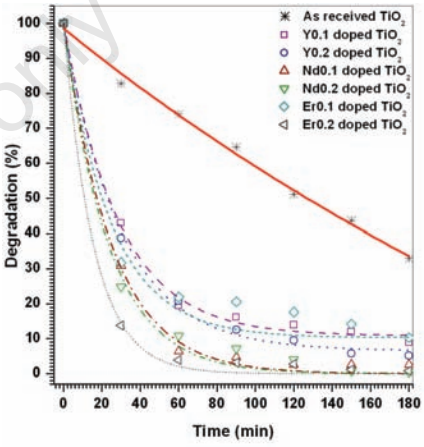

Figure 6. Photocatalytic degradation of CR in the presence of Nd^{3+} and Er^{3+} doped TiO_2 NC samples. For comparison, the results obtained with Y^{3+} doped TiO_2 NCs (9) are also shown.

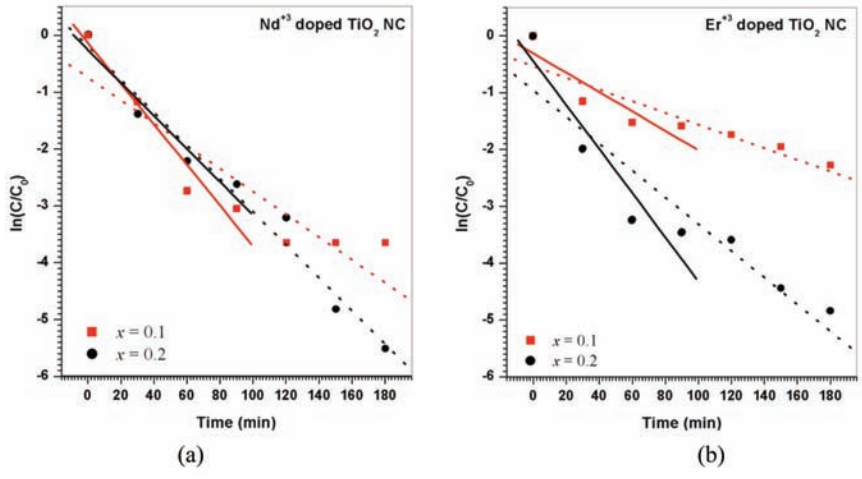

Figure 7. Plots of $\ln(C/C_0)$ against time with the best-fitting straight lines. The slopes of these lines give the rate constant. Solid line, best fit to first four points; dotted line, best fit to all points.

those reported for pure anatase nanodots[12] in terms of their C'_{180} and k_{obs} as estimated by Narayan *et al.*[9] For the 10 and 15 nm nanodots, the estimated values for C'_{180} were 60 and 70%, and that of k_{obs} were 0.05×10^{-2} min^{-1} and 0.07×10^{-2} min^{-1}, respectively[9] for degradation under UV-A source of wavelength 350 nm (emission maximum).[12] Such small degradations, even though the experimental conditions were different, may be due to the high rate of e^-/h^+ recombination in the undoped samples. Additionally, the spherical nanodots would definitely have smaller specific surface area as compared to any other shape, which may also be responsible for the relatively low degradation through photosensitization.

The doping of TiO_2 with Nd^{3+} and Er^{3+} ions marginally modifies the band-gaps even though the corresponding oxides have wider band gaps of 4.7 and 5.3 eV, respectively. Relative to pure TiO_2 (λ_{cutoff} = 390 nm), the red-shift of absorption edge due to doping was only up to a maximum of 422 nm (observed with x=0.2 Er^{3+} doping). As mentioned before, since the source of light emitted λ>420 nm, these small band-gap modifications may not be of much significance as far as the present degradation experiments are concerned. However, as seen from the absorption spectra of the NCs, apparently some new energy levels were introduced due to the doping of Nd^{3+} and Er^{3+} ions, which might contribute to photocatalysis. Keeping these points in mind, another comparison of observed results in a slightly different way can shed some light on the role of DWF. To make these comparisons, we considered those NCs that have nearly identical particle size. The x=0.1 Nd^{3+} doped NC had an average particle size of 13 nm, which is close that of 12 nm for x=0.2 Er^{3+} doped NC. Respectively, C'_{180}=97% and $k_{obs}=2.01\times10^{-2}$ min^{-1} and C'_{180}=99% with $k_{obs}=2.36\times10^{-2}$ min^{-1} were observed with these NCs. In this pair, the marginally better performance of Er^{3+} doped NC may be easily attributed to a higher DWF (=55%) as compared to that in the Nd^{3+} doped NC (DWF=32%). This inference is further consolidated when the x=0.2 Nd^{3+} doped NC (15 nm particle size) is compared with x=0.1 Er^{3+} doped NC (16 nm). Even with nearly the same particle size, the Nd^{3+} doped NC degraded close to 100% of CR (C'_{180}) at a much higher $k_{obs}=2.91\times10^{-2}$ min^{-1}, as against C'_{180}=90% and $k_{obs}=1.03\times10^{-2}$ min^{-1} of Er^{3+} doped NC. The reason becomes clear when their respective DWF of 51% and 35% are noted. Furthermore, one of our previously reported[9] results with Y^{3+} doped (x=0.1) NC that had 16 nm of average particle size, but only about 24% of DWF, also falls in line with these observations. The Y^{3+} doped NC had degraded only about 91% of CR in 180 min (C'_{180}), although with a higher rate of $k_{obs}=2.74\times10^{-2}$ min^{-1}.

It is quite evident from this discussion that the presence of a higher concentration of suitable dopant ions (higher DWF) may support the photocatalytic degradation. As a final point, we discuss the mechanism that may be associated with the process of photocatalysis in these and similar composite materials. Expectedly, the dopants support the enhancement of degradation in two ways: i) through an efficient suppression of e^-/h^+ recombination, and ii) by the introduction of intermediate energy states in the energy gap of the host TiO_2, which may facilitate visible light sensitivity of the composites. It is noteworthy to mention here that both of these favorable events may progress through the same basic mechanism. Electron-trapping properties of rare-earth ions are well known.[17,18] It has been reported that doping of Yb^{3+} ions in InP creates an iso-electronic acceptor-like energy level at 30 meV below the CB of the semiconductor. Similar levels may be introduced in any semiconductor through the doping of rare-earths because of the similarity of the electronic structure of the latter.[25] These intermediate, rare-earth related energy levels may not only act as electron-traps, but they could also facilitate the absorption of visible radiations through indirect narrowing of the band gap. Upon irradiation with visible light, the electrons produced in the molecules (pollutant) adsorbed on the TiO_2 particles can be captured on these traps, and thus the holes would be left alone to freely participate in the chemical processes leading to degradation (suppression of e^-/h^+ recombination). Moreover, the electrons in the VB of TiO_2 would require less energy to get excited to the rare-earth related intermediate energy level, which may be supplied through visible light irradiation, and thus photocatalytic degradation through the process of photo-excitation may also be initiated.

Conclusions

In the recent past, rare-earth ions have been identified as suitable doping agents to improve the photocatalytic degradation efficiency of TiO_2. Through the process of photosensitization, which is supported by smaller particle size (larger specific surface area), the rare-earth ions doped TiO_2 composites can produce significant degradation under visible light irradiation. In this article, we have reported the visible light photocatalytic activity of Nd^{3+} and Er^{3+} doped TiO_2 composites, $TiO_2[R_2O_3]_x$ {x=0.1, 0.2; R≡Nd, Er}, in the degradation of Congo red dye. NCs with molar concentration x=0.2 of both doping types have produced close to 100% degradation at excellent rates. The other composition of NCs with x=0.1 also showed reasonably significant degradation of CR. The observations have been attributed to the smaller particle size (12-16 nm) of the NCs, as well as to an appropriate weight fraction of the rare-earth dopants in the composites. Doping of rare-earth ions may introduce intermediate energy levels between the VB and CB of the host TiO_2 which may act like efficient electron traps for suppression of the unwanted e^-/h^+ recombination. At the same time, these energy levels could also help in narrowing down the energy gap indirectly, such that visible light-induced photocatalysis becomes possible through photo-excitation.

As far as the possible practical applications are concerned, these NC materials may be deposited as thin-films on transparent substrates. Using these thin-films, a special photo-reactor may be fabricated for the treatment of continuously flowing waste water. Since these photocatalysts are sensitive to visible wavelengths, the sunlight may possibly be used for irradiation. More work in this direction is in progress.

References

1. Wambuguh D, Chianelli RR. Indigo dye waste recovery from blue denim textile effluent: a by-product synergy approach. New J Chem 2008;32:2189-94.
2. Gharbani P, Tabatabaii SM, Mehrizad A. Removal of Congo red from textile wastewater by ozonation. Int J Environ Sci Tech 2008;5:495-500.
3. Bergamini RBM, Azevedo EB, Raddi de Araújo LR. Heterogeneous photocatalytic degradation of reactive dyes in aqueous TiO2 suspensions: decolorization kinetics. Chem Eng J 2009;149:215-20.
4. Tapalad T, Neramittagapong A, Neramittagapong S, Boonmee M. Degradation of Congo red dye by ozonation. Chiang Mai J Sci 2008;35:63-8.
5. Fabbri D, Prevot AB, Pramauro E. Effect of surfactant microstructures on photocatalytic degradation of phenol and chlorophenols. Appl Catal B Environ 2006;62:21-7.
6. Linsebigler AL, Lu G, Yates JT Jr. Photocatalysis on TiO2 surfaces: Principles, mechanisms, and selected results. Chem Rev 1995;95:735-58.
7. Hashimoto K, Irie H, Fujishima A. TiO2 photocatalysis: A historical overview and future prospects. Jpn J Appl Phys 2005;44:8269-85.
8. Bumpas JA, Tricker J, Andrzejewski K, et al. Remediation of water contaminated with an azo dye: An undergraduate laboratory experiment utilizing an inexpensive

photocatalytic reactor. J Chem Edu 1999;76:1680-3.
9. Narayan H, Alemu HM, Macheli L, et al. Synthesis and characterization of Y3+-doped TiO2 nanocomposites for photocatalytic applications. Nanotechnology 2009;20:255601.
10. Narayan H, Alemu HM, Macheli L, et al. Role of particle size in visible light photocatalysis of Congo red using TiO2 [ZnFe2O4]x nanocomposites. Bull Mater Sci 2009;32:499-506.
11. Yao Y, Li G, Ciston S, et al. Photoreactive TiO2/carbon nanotube composites: Synthesis and reactivity. Environ Sci Technol 2008;42:4952-7.
12. Wahi RK, Yu WW, Liu Y, et al. Photodegradation of Congo red catalyzed by nanosized TiO2. J Molecular Catal A Chem 2005;242:48-56.
13. Liqiang J, Xiaojun S, Baifu X, et al. The preparation and characterization of La doped TiO2 nanoparticles and their photocatalytic activity. J Solid State Chem 2004;177:3375-82.
14. Li Z, Shen W, He W, Zu X. Effect of Fe-doped TiO2 nanoparticle derived from modified hydrothermal process on the photocatalytic degradation performance on methylene blue. J Hazard Mater 2008;155:590-4.
15. Vogel R, Pohl K, Weller H. Sensitization of highly porous, polycrystalline TiO2 electrodes by quantum sized CdS. Chem Phys Lett 1990;174:241-6.
16. Ashokkumar M, Kudo A, Saito N, Sakata T. Semiconductor sensitization by RuS2 colloids on TiO2 electrodes. Chem Phys Lett 1994;229:383-8.
17. Xie Y, Yuan C. Characterization and photocatalysis of Eu3+–TiO2 sol in the hydrosol reaction system. Mater Res Bull 2004;39: 533-43.
18. Liu J, Yang R, Li S. Synthesis and photocatalytic activity of TiO2/V2O5 composite catalyst doped with rare earth ions. J Rare Earths 2007;25:173-8.
19. Jia XL, Wang Y, Xin RS, et al. Preparation of rare-earth element doped titanium oxide thin films and photocatalysis properties. Key Eng Mater 2007;336-338:1946-8.
20. El-Bahy ZM, Ismail AA, Mohamed RM. Enhancement of titania by doping rare earth for photodegradation of organic dye (Direct Blue). J Hazard Mater 2009;166: 138-43.
21. Yang X, Zhu L, Yang L, et al. Preparation and photocatalytic activity of neodymium doping titania loaded to silicon dioxide. Trans Nonferrous Met Soc China 2011;21: 335-9.
22. Xie Y, Yuan C. Photocatalysis of neodymium ion modified TiO2 sol under visible light irradiation. Appl Surf Sci 2004;221: 17-24.
23. Zhang WF, He YL, Zhang MS, et al. Raman scattering study on anatase TiO2 nanocrystals. J Phys D Appl Phys 2000;33: 912-6.
24. Šćepanović MJ, Grujić-Brojčin M, Dohčević-Mitrović ZD, Popović ZV. Characterization of anatase TiO2 nanopowder by variable-temperature Raman spectroscopy. Sci Sintering 2009; 41:67-73.
25. Klik MAJ, Gregorkiewicz T, Bradley IV, Wells JPR. Optically induced deexcitation of rare-earth ions in a semiconductor matrix. Phys Rev Lett 2002;89:227401.